8th Biennial International Conference
& Exposition on Petroleum Geophysics

"HYDERABAD 2010"

**P-106**

# Global 4-D Seismic Inversion and Fluid Prediction

***Y. Lafet, B. Roure, P.M. Doyen, R. Bornard, H. Buran, A. Smith****, CGGVeritas*

***Summary***

*Independent inversion of base and monitor seismic surveys can yield estimates of elastic properties that are inconsistent with expected production effects. We therefore propose a global time-lapse inversion scheme, involving joint inversion of base and monitor data. All vintages and input angle stacks are combined in a single objective function, which is optimized using simulated annealing to estimate the time-variant distribution of elastic attributes that best matches all available data. The multi-vintage nature of the optimization allows us to incorporate flexible, user-defined rock physics constraints on the evolution of $V_p$, $V_s$ and density between consecutive surveys. There are no restrictions on the number of input angle stacks or number of monitor surveys. The constrained, global inversion solution can therefore be easily updated as new data become available. We apply the global 4-D inversion with rock physics coupling to data from the Brage Field and compare results with a workflow involving separate inversion of base and monitor data. The global 4-D inversion results are combined with a time-lapse Bayesian fluid classification scheme to map production-induced fluid movement and quantify associated uncertainty.*

## Introduction

Time-lapse seismic analysis now plays an important role in reservoir management. As the technology matures, there is an increased emphasis on quantitative 4-D interpretation workflows, involving 4-D elastic inversion followed by rock physics inversion to estimate changes in fluid saturation and reservoir pressure. Obtaining reliable estimates of time-lapse changes in elastic properties using 4-D seismic inversion is a challenging task which has received considerable attention in the last few years. A number of 4-D inversion approaches have been proposed (Sarkar et al., 2003), including 1) workflows where base and monitor surveys are inverted separately and then differenced to calculate changes in elastic attributes, 2) sequential inversion schemes where inversion results for a base survey are used to define an initial model for inverting a monitor survey (e.g., Lafet et al., 2005), 3) direct inversion of amplitudes differences for changes in elastic parameters (e.g., Buland and El Ouair, 2006) and 4) global inversion methods where all vintages are inverted simultaneously (e.g., El Ouair and Strønen, 2006). Experience shows that coupling the inversion of base and monitor surveys is important to obtain quantitative estimates of impedance changes and reduce the non-uniqueness of the inversion process. Here we present a new global inversion scheme where all data vintages are inverted simultaneously. Inversion coupling between successive surveys is achieved using rock physics constraints, honouring expected production effects. We illustrate the global 4-D inversion scheme using time-lapse seismic data from the Brage Field and show the benefits of the new approach compared to independent inversion of base and monitor data. From the 4-D inversion results, we map changes in hydrocarbon distribution using a time-lapse Bayesian fluid classification procedure.

## Global 4-D Inversion Methodology

The new algorithm extends the 3-D simultaneous elastic inversion method described by Coulon et al. (2006) to joint multi-vintage inversion, with simultaneous inversion of all angle stacks for base and monitor surveys, as illustrated schematically in Figure 1. The multi-vintage, global inversion starts from an initial layered model defined for P-wave velocity, $V_p$, S-wave velocity, $V_s$ and density, $\rho$ at each survey time. The initial model is constructed using a

stratigraphic grid framework defined in the time domain. In the vertical direction, grid cell thicknesses vary typically between 4 and 6 msec. Laterally, grid cell dimensions are fixed by the seismic trace spacing. The structure of the grid is the same for each survey time. This allows us to control the time evolution of the elastic properties ($V_p$, $V_s$ and $\rho$) cell-by-cell during the 4-D inversion process. Furthermore, we can modify the time thickness of the grid cells to reflect changes in cell velocities due to production.

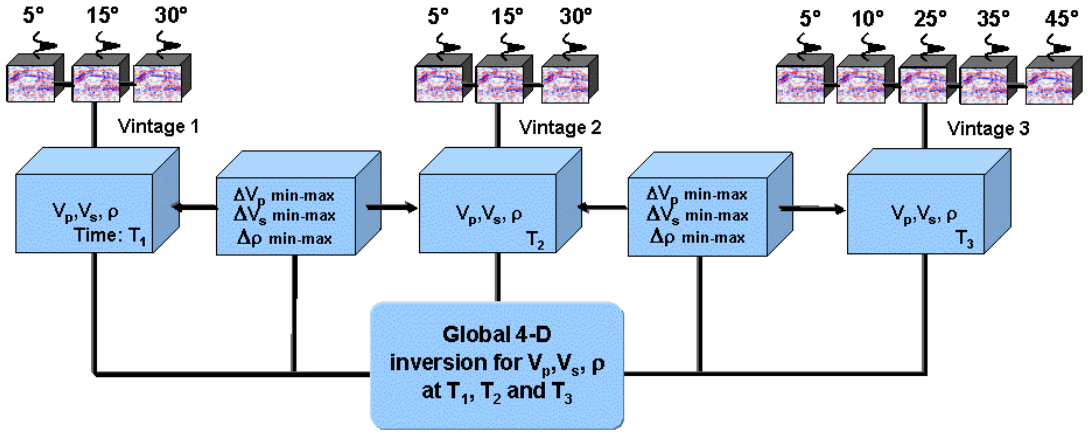


Figure 1: Global inversion of multiple seismic vintages and angle stacks with 4-D corridor constraints for coupling inverted attributes between successive surveys. A wavelet is input for each partial stack.

During inversion, the time-dependent initial model is iteratively perturbed to find a global solution that optimizes simultaneously the match between the input angle stacks for all vintages and the corresponding synthetics, calculated by wavelet convolution with full Zoeppritz reflectivity equations or Aki-Richards equations depending on the maximum angle. The optimized multi-vintage cost function combines several terms such as the level of residual energy for each angle stack and each vintage, the distance from the initial model and multi-trace lateral continuity constraints. The cost function is minimized using a Simulated Annealing (SA) procedure that is adapted to the multi-vintage setting and allows user control on the level of 4-D coupling between inverted elastic attributes. During the SA process, joint perturbations of $V_p$, $V_s$ and $\rho$ values are introduced for the base and all monitor surveys, and are accepted or rejected as a whole. Time-lapse coupling is achieved by restricting the range of the perturbations between successive surveys according to user-specified constraints. Specifically, between each consecutive vintage, perturbations are restricted to lie in specific min-max intervals; this limits the range of values explored by the SA algorithm. For example, if water injection takes place between the base and monitor survey times, we may expect a large increase in $V_p$ but only a small decrease in $V_s$ due to density change. This information is easily incorporated in the form of 4-D interval constraints. The user-defined bounds are both space-variant and time-variant, and are specified as 4-D cubes of min and max values for each inverted attribute. In practice, selection of the perturbation corridors will depend on a number of factors such as the degree of confidence in the initial model, the reliability of the rock-physics information linking successive surveys, the magnitude of the 4-D signal and other geological interpretation constraints. For example, zero-width 4-D corridors may be imposed in cells of the layered model that are known to be non-reservoir and where no production effects are expected. In these cells, a time-invariant model optimization is performed across all vintages, hence reducing the impact of non-repeatable noise on inversion results. The 4-D coupling introduced in our global, multi-vintage inversion scheme reduces the inversion non-uniqueness and allows us to identify solutions that are consistent with basic rock physics information.

**4-D Inversion Case Study**

We performed a global 4-D inversion using seismic data from the Brage Field, Norwegian North Sea. The goal was to help identify undrained hydrocarbon sands in the Lower Jurassic Statfjord Formation, in production since 1993. The Statfjord Formation consists of a thick, sand-dominated package of fluvial channel sandstones and fine-grained overbank deposits. The Brage Statfjord reservoir is located in a horst block bounded by major faults, with throw in excess of 200m. Reservoir thickness ranges between 80m and 100m. A NW-SE trending fault transects the horst structure and defines two reservoir compartments. In each block, pressure is maintained by water injection and oil was produced from 6 wells in 2003 at the time of the 4-D acquisition; eight wells are now producing in 2007. Seismic data acquired in 1992 and 2003 have been recently reprocessed using a PSDM workflow (Kvalheim et al., 2007), resulting in 6 partial stacks for each survey, with angles ranging between $4^o$ and $40^o$. The large vertical movement of the oil-water contact due to 10 years of production gives rise to a prominent 4-D signal, which must be interpreted to help locate and quantify the volume of remaining "attic" oil. Quantitative 4-D interpretation is rendered difficult by the presence of multiples at the target level, which corrupt the seismic response.

Following independent wavelet extraction for each vintage and each angle stack, and time-alignment of all data cubes, we inverted base and monitor surveys simultaneously, using 4-D constraint cubes for time-lapse coupling between inverted parameters. We first defined a "4-D mask" by thresholding a filtered energy attribute cube, computed from 2003-1992 amplitude differences. All cells from the layered model located outside the mask (i.e., with low energy difference values) were assigned a zero-width 4-D interval constraint, implying that inverted properties are forced to have the same values at base and monitor survey times. Inside the 4-D mask, the allowed ranges of $\Delta V_p$, $\Delta V_s$ and $\Delta\rho$ between base and monitor surveys were determined from fluid substitution analysis: water injection is expected to increase $V_p$ and $\rho$ by a maximum of 5% and decrease $V_s$ by up to 2%. Pressure effects on the 4-D response are expected to be very small and were therefore not included in the definition of the 4-D corridor constraints.

Figure 2 shows the 4-D inversion results at vertical exploration well 31-4-8. The two tracks on the left compare the log values (black) of P-wave and S-wave impedance ($I_p$ and $I_s$) with the corresponding inverted values for the base

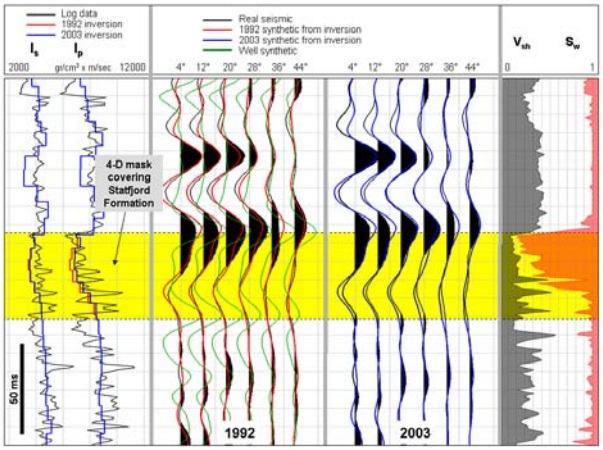


Figure 2: Global 4-D inversion results at well 31-4-8.

(red) and monitor (blue) surveys. The band coloured in yellow corresponds to the 4-D mask, which at this location, spans the entire Stafjord interval. We only allow time-lapse variations in inverted acoustic impedance inside the 4-D mask. Hence, the blue and red curves differ only in the reservoir zone, where a slight increase of $I_p$ is observed from 1992 to 2003, due to water influx. In the same figure, the seismic traces panel compares synthetic and real amplitudes for base and monitor surveys for the different angle stacks, together with the seismic response computed from the sonic log data. The match between real amplitudes and synthetic amplitudes computed from the inversion results is good but the match with the well synthetics is poor, especially for the near angles. This discrepancy is due to the effects of residual multiples energy at the target level.

The $\Delta I_s$ vs $\Delta I_p$ cross plots in Figure 3 compare the results of global 4-D inversion (b) with independent inversions of the base and monitor surveys (a). In the independent inversion workflow, base and monitor data were inverted separately, starting from the same initial model. Only the cross plot (b), which corresponds to the global inversion, is consistent with the expected effect of water flooding: a relatively large $I_p$ increase and a much smaller increase in $I_s$. Due to the lack of 4-D coupling between inverted parameters, independent inversion yields spurious negative $\Delta I_s$ and $\Delta I_p$ values,

inconsistent with the hypothesis that water is replacing oil. Inversion amplitude residuals depicted in the same figure show the similar energy level for both independent and global 4-D inversions. This demonstrates the non-unique nature of the inversion and the importance of introducing 4-D constraints to find physically consistent solutions.

**4-D Interpretation of Fluid Movements**

The results of the global 4-D inversion were interpreted in terms of production-induced fluid movements in the Statfjord reservoir using a time-lapse supervised Bayesian classification procedure. Three litho-classes ($C_i$, i=1, …, 3) were considered in the 4-D classification: oil-sand, water-sand and shale. For each class, a training set of $I_p$ and $I_s$ values was constructed by extracting inverted attributes from the pre-production 1992 survey around two exploration well locations with known lithologies over the Statfjord interval. The impedance cross-plot in Figure 4 (a) shows the training set for

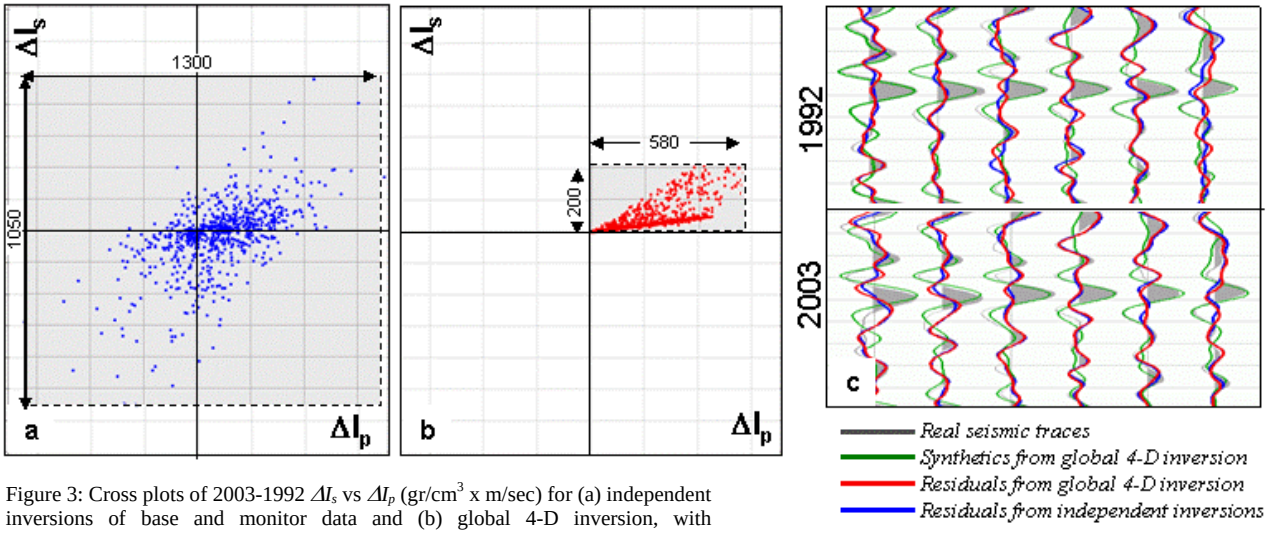


Figure 3: Cross plots of 2003-1992 $\Delta I_s$ vs $\Delta I_p$ (gr/cm$^3$ x m/sec) for (a) independent inversions of base and monitor data and (b) global 4-D inversion, with corresponding amplitude residuals in (c). Data points correspond to the Statfjord interval.

each litho-class, together with the corresponding class-conditional impedance Probability Distribution Functions (PDFs), $p(I_p, I_s \mid C_i)$, constructed using the non-parametric kernel density estimation technique (Silverman, 1986). The impedance PDFs for water-sand and shale overlap significantly but there is a good separation with the oil-sand class. After the training phase, the different litho-probabilities, $p(C_i \mid I_p, I_s)$, were computed at each point from the inverted attributes. The litho-probability cubes were calculated independently from the base and monitor inversions using the same attribute PDFs. Figure 4 (b to e) shows the time evolution of the oil-sand probabilities from 1992 to 2003. The vertical sections and stratigraphic maps clearly depict the change in fluid distribution after 10 years of production and are broadly consistent with expected effects of the water flood.

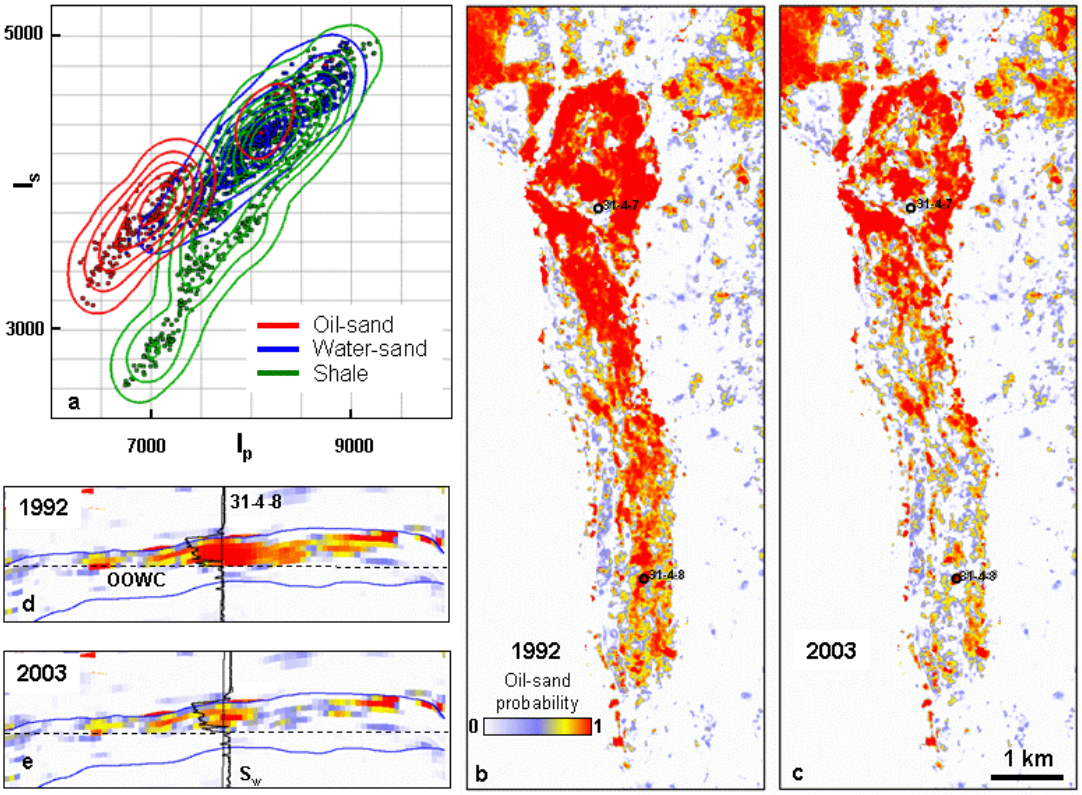


Figure 4: Results of time-lapse Bayesian fluid classification: (a) impedance [gr/cm$^3$ x m/sec] PDFs computed from 5x5 inverted traces around two vertical wells, (b) and (c) 1992 and 2003 oil-sand probability maps near top reservoir, (d) and (e) 1992 and 2003 oil-sand probability E-W sections at well 31-4-8.

## Conclusions

Time-lapse seismic inversion is inherently non-unique. It is therefore important to constrain the inversion process to obtain solutions consistent with rock physics information. Joint inversion of base and monitor data allows us to constrain the time evolution of inverted elastic attributes with simple rock physics rules restricting the range of variations between consecutive surveys. For the Brage case study, constrained, global 4-D inversion yields impedance estimates that are more consistent with the expected effects of the water flood, compared to our separate inversions of base and monitor surveys. Time-lapse Bayesian fluid classification of the inverted attributes allows us to map production-induced fluid movement and evaluate uncertainty in 4-D fluid discrimination.

## Acknowledgements

The authors would like to thank StatoilHydro for permission to present this paper.

## Technical References

Buland, A. and El Ouair, Y., Bayesian time-lapse inversion, 2006, Geophysics, Vol. 71, 3, R43-R48.

Coulon, J.-P., Lafet, Y., Deschizeaux, B., Doyen, P.M. and Duboz, P., 2006, Stratigraphic elastic inversion for seismic lithology discrimination in a turbiditic reservoir, SEG Expanded Abstract, 2092-2096.

El Ouair, Y., and Strønen, L., 2006, Value creation from 4D seismic at the Gullfaks Field: achievements and new challenges, SEG Expanded Abstract, 3250-3254.

Kvalheim, A.K. Sandø, I.A., Skogland, S.M., Vinje V. and Carpenter, M., 2007, Impact of time and depth imaging methods on quantitative 4D reservoir management, 69th EAGE Conference& Exhibition, Madrid, Expanded Abstract H017.

Lafet, Y., Duboz, P., Deschizeaux, B., Lefeuvre, F., and Hubans, C., 2005, 4D Stratigraphic inversion of the Girassol field – Towards a more quantitative approach, 67th EAGE Conference and Technical Exhibition, Madrid, Expanded Abstract C018.

Sarkar, S., Gouveia, W.P. and Johnston, D.H., 2003, On the inversion of time-lapse data, SEG Expanded Abstract, 1489-1492.

Silverman, B.W., 1986, Density estimation for statistics and data analysis, Chapman & Hall, 175p.